Graph Laplacian Spectrum of Structural Brain Networks is Subject-Specific, Repeatable but Highly Dependent on Graph Construction Scheme

Stavros I Dimitriadis[1-8], Eirini Messaritaki [3,4,5], Derek K Jones [3,5]

[1]Department of Clinical Psychology and Psychobiology, Faculty of Psychology, University of Barcelona, Passeig de la Vall d'Hebron, 171, 08035, Barcelona, Spain
[2]Institut de Neurociències, University of Barcelona, Campus Mundet, Edifici de Ponent , Passeig de la Vall d'Hebron, 171, 08035 , Barcelona, Spain
[3]*Cardiff University Brain Research Imaging Centre (CUBRIC), School of Psychology, Cardiff University, Maindy Road, Cardiff (Wales), CF24 4HQ, UK*
[4]*Division of Psychological Medicine and Clinical Neurosciences, School of Medicine, Cardiff University, Cardiff (Wales), CF24 4HQ, UK*
[5]*School of Psychology, Cardiff University, 70 Park Place, Cardiff (Wales), CF10 3AT, UK*
[6]*Neuroinformatics Group, Cardiff University Brain Research Imaging Centre, School of Psychology, Cardiff University, Cardiff (Wales), , CF24 4HQ, UK*
[7]*Integrative Neuroimaging Lab, 55133 Thessaloniki, Makedonia, Greece*
[8]*Neuroscience and Mental Health Research Institute, Cardiff University, Cardiff (Wales), United Kingdom*
[9]*MRC Centre for Neuropsychiatric Genetics and Genomics, School of Medicine, Cardiff University, Cardiff (Wales), United Kingdom*

Corresponding author:

Stavros I. Dimitriadis

Contact: DimitriadisS@cardiff.ac.uk / stidimitriadis@gmail.com

Department of Clinical Psychology and Psychobiology, Faculty of Psychology, University of Barcelona, Passeig de la Vall d'Hebron, 171, 08035, Barcelona, Spain

Abstract:

The human brain is a complex network that can be summarized as a graph where nodes refer to anatomical brain regions while edges encode the neuronal interactions or structural connections between them at both the micro and macroscopic levels, allowing the application of graph theory to investigate the network brain architecture. Various network metrics have been proposed and adopted so far describing both local and global properties of the relevant brain network. It has been proposed that connectomic harmonic patterns that emerged from the brain's structural network underlie the human brain's resting-state activity. Connectome harmonics refer to Laplacian eigenfunctions of the structural connectivity matrices (2D) and is an extension of the well-known Fourier basis of a signal (1D). The estimation of the normalized graph Laplacian over a brain network's spectral decomposition can reveal the connectome harmonics (eigenvectors) corresponding to certain frequencies (eigenvalues). Here, we used test-retest dMRI data from the Human Connectome Project to explore the repeatability of connectome harmonics and eigenvalues across five graph construction schemes. Normalized Laplacian eigenvalues were found to be subject-specific and repeatable across the five graph construction schemes, but their range is highly dependent on the graph construction scheme. The repeatability of connectome harmonics is lower than that of the Laplacian eigenvalues and shows a heavy dependency on the graph construction scheme. In parallel, we investigated the properties of the structural networks and their relationship with the Laplacian spectrum. Our results provide a proof of concept for repeatable identification of the graph Laplacian spectrum of structural brain networks based on the selected graph construction scheme.

Keywords: brain network, connectome, Laplacian, eigenvalues, graph spectrum, normalized Laplacian, diffusion magnetic resonance imaging, structural brain network

1. Introduction

The human brain can be modeled as a graph $G = (V, E)$, comprising of nodes, V, representing brain regions and edges, E, referring to functional and anatomical strengths (Bullmore and Sporns, 2012). A high repertoire of network metrics has been adopted from social network analysis and applied to the analysis of human brain networks. Those metrics quantify different global and local properties of nodes such as the degree, the communication efficiency, etc (Boccaletti et al., 2006; Newman, 2003). Complementary to trivial network metrics, researchers have proposed a variety of qualitative measures for the examination of the global structure of brain networks (Atay et al., 2006; Banerjee and Jost, 2007; Banerjee, 2012; Varshney et al., 2011).

The eigenanalysis of the graph Laplacian operator over the structural brain network reveals a set of graph Laplacian eigenvectors and eigenvalues. The graph Laplacian eigenvectors, called connectome harmonics, is a set of frequency ordered harmonic patterns arising from the cortex and can be seen as a connectome extension of the well-known Fourier basis of a 1D signal to the 2D human brain network. These connectome harmonics reported a relationship between low-frequency harmonics (eigenvectors linked to smaller Laplacian eigenvalues) and the resting-state brain activity mainly from the default mode network (DMN) measured by functional magnetic resonance imaging (fMRI) recordings (Atasoy et al., 2016, 2018b).

The transformation of the original brain network to the normalized Laplacian matrix gives us the opportunity to estimate the Laplacian eigenvalues which refer to the global network structure (Banerjee, 2012; Chung, 1996). The advantage of the normalized Laplacian spectrum over unnormalized is that all the relevant eigenvalues range between 0 and up to a maximum of 2, which further enables the comparison of networks across modalities, cohorts, age groups, and even sizes (Banerjee, 2012).

Research studies have applied spectral graph theory to neural networks (Banerjee and Jost, 2007; Varshney et al., 2011), proposing network metrics tailored to the eigenvectors of the brain network, the node centrality (Bonacich, 2007, 1972; Page et al., 2001) and community detection methods (Fortunato, 2010; Harriger et

al., 2012; Liang et al., 2011; Newman, 2006). The eigenvectors of a network are related to the local properties of a node over its neighborhood while the associated eigenvalues contain important information about the graph structure (Banerjee and Jost, 2007; Banerjee, 2012; McGraw and Menzinger, 2008; Vukadinović et al., 2002).

Many researchers have already applied the graph Laplacian to brain connectivity networks reporting the progression of neurodegenerative diseases (Raj et al., 2012), brain malformation (Wang et al., 2017), attention switching period in a cognitive task (Huang et al., 2018; Medaglia et al., 2018), macroscale coupling gradient between brain regions (Preti and Van De Ville, 2019), structure-function decoupling (Griffa et al., 2022), and an aberrant dynamic connectivity profile constrained by structural brain network in patients with concussion (Sihag et al., 2020). These studies focus on long-range and white-matter-based anatomical connectivity employing brain networks of sizes from a few tens up to a few hundred regions-of-interests (ROI) (Desikan et al., 2006; Destrieux et al., 2010). Recently, Atasoy et al. proposed an alternative framework for the application of the graph Laplacian to analysis of the human connectome. They combined assessment of local connectivity of the gray matter cortical structure captured from the magnetic resonance imaging (MRI) data with the assessment of long-range connectivity mediated via the white-matter thalamocortical fibers captured from the diffusion MRI (dMRI) data into a common anatomical network without the use of a template (Atasoy et al., 2017, 2016; Naze et al., 2021).

The analysis of the relation between the spectrum of a graph, i.e., the eigenvalues of its adjacency matrix, and the structure of the graph is the main goal of spectral graph theory. The general theme was then, firstly, to compute the eigenvalues of such matrices, and secondly, to relate the eigenvalues to structural properties of graphs. In the present study, we investigated the repeatability of the Laplacian eigenvalue spectrum and the Laplacian eigenvectors (connectome harmonics) of the structural brain networks derived from dMRI. We analyzed the test-retest MRI and diffusion-MRI data set from the multimodal neuroimaging database of the Human Connectome Project (HCP) (Glasser et al., 2013; S N Sotiropoulos et al., 2013; Van Essen et al., 2013). Additionally, we studied specific topological properties of a network like the number of modules, structural motifs, and bipartiteness of the SBN reflected in the Laplacian Spectrum while we demonstrated their relationship.

The main aims of the present study are the following :

1) to shed light on the relationship of the Laplacian spectrum of a SBN with specific structural topological properties of the SBN
2) to reveal their relationship
3) to explore the repeatability and individuality of both the Laplacian spectrum and the relevant structural properties of the SBN
4) to investigate how all the aforementioned three aims are influenced by the graph construction scheme

The rest of this manuscript is organized as follows: Section 2 (Methods) describes briefly the cohort, the graph construction schemes, and the estimation of the normalized Laplacian matrix. Section 3 (Results) reports our findings in terms of repeatable normalized Laplacian eigenvalues and eigenvectors and their subject specificity under the brain fingerprinting framework. Section 4 (Discussion) summarises the major contribution of our study explaining its advantages, limitations, and possible future directions.

2. Methods

All analyses were performed using MATLAB (2019a; The Mathworks, Inc., MA).

2.1. Data

Our study adopted the test-retest MRI and diffusion-MRI dataset from the large multimodal neuroimaging database of the Human Connectome Project (HCP) (Glasser et al., 2013; S N Sotiropoulos et al., 2013; Stamatios N Sotiropoulos et al., 2013; Van Essen et al., 2013). The cohort used in our study consists of 37 subjects which were scanned twice with a time interval between the scans ranging between 1.5 and 11 months. The age range of the participants was 22–41 years. It should be noted that the test-retest time interval is shorter than the expected time over which maturation-induced structural changes can be measured with the diffusion MRI (dMRI) experiment reported in this study.

The diffusion-weighted images (DWIs) had a resolution of (1.25×1.25×1.25) mm^3 and were acquired at three different diffusion weightings (*b*-values: 1000□s/mm^2, 2000□s/mm^2 and 3000□s/mm^2) across 90 gradient orientations for each *b*-value.

The HCP acquisition details and pre-processing are described in (Feinberg et al., 2010; Glasser et al., 2013; Moeller et al., 2010; Setsompop et al., 2012; S N Sotiropoulos et al., 2013; Stamatios N Sotiropoulos et al., 2013; Xu et al., 2012). Our previous studies used the same cohort (Dimitriadis et al., 2021; Messaritaki et al., 2019). We performed the following analyses using the b=2000 s/mm^2 data (this value chosen versus the other two because it gives reliable tractography results with the CSD algorithm *and* reliable results for the DT fits).

2.2. Tractography

We performed whole-brain tractography employing ExploreDTI-4.8.6 (Leemans et al., 2009) as in our previous studies (Dimitriadis et al., 2021; Messaritaki et al., 2019). We estimated the fiber orientation distribution function (fODF) using constrained spherical deconvolution (CSD) (Tournier et al., 2004) (Tournier et al., 2004). Tracking was initiated on a 2×2×2 mm grid, with a 1 mm step size, an angular threshold of 30°, and a fiber length range of 50−500 mm.

2.3. Graph generation

2.3.1. Node definition

As in our previous studies, we adopted the Automated Anatomical Labeling (AAL) atlas (Tzourio-Mazoyer et al., 2002) to define 90 cortical and subcortical areas (45 areas per hemisphere) as nodes of the constructed structural brain graphs. Structural brain networks (SBN) were generated for each participant and for each edge weight (see section 2.3.2) using ExploreDTI-4.8.6 (Leemans et al., 2009).

2.3.2. Edge weights

We weighted the edges of the SBN by adopting the five most repeatable graph-construction schemes revealed previously with the same dataset (Messaritaki et al., 2019b), which were based on alternative combinations of the nine metrics listed in Table 1 (see Section 2.3.4). The edge weights of every SBN were normalized to have a maximum edge weight of 1, while the elements in the main diagonal were set to zero.

Table 1. Metrics used in connectivity matrices.

Metric	Abbreviation
Fractional anisotropy	FA
Mean diffusivity	MD
Radial diffusivity	RD
Number of streamlines	NS
Percentage of streamlines	PS
Streamline density	SLD
Tract volume	TV
Tract length	TL
Euclidean distance between nodes	ED

2.3.3 Integrated Edge-Weights

Each metric shown in Table 1 conveys different information regarding the tissue properties. We previously proposed an integrated edge weighting scheme combining the metric-based SBN under a data-driven whole-brain algorithm (Dimitriadis et al., 2017a,b,c). An integrated SBN was formed by the combination of the nine metric-based SBNs for every participant and scan session.

An orthogonal-minimal-spanning-tree (OMST) algorithm was applied to every metric-based SBN, selecting edges of both small and large weights that preserved

the efficiency of brain regions at a minimal wiring cost. The overall algorithm with the OMST on its center down-weights the metrics with a higher global topological similarity and up-weights the dissimilar metrics enhancing the complementarity of topological information across the nine adopted metrics. More details on the OMST algorithm and its implementation can be found in our previous work (Dimitriadis et al., 2017b, 2017c) (Dimitriadis et al., 2021, 2017a; Messaritaki et al., 2019) and the related code is freely available at https://github.com/stdimitr/multi-group-analysis-OMST-GDD.

2.3.4 Graph Construction Schemes

We will briefly explain the five graph construction schemes used here as in our previous studies (Dimitriadis et al., 2021; Messaritaki et al., 2019).

The first category includes SBN constructed via the data-driven algorithm (Dimitriadis et al., 2017b, 2017a, 2017c).

A) NS-OMST: apply the OMST filtering algorithm (Dimitriadis et al., 2017b, 2017a, 2017c) to the NS-weighted matrix.

B) 9m-OMST: Integrate all nine diffusion metrics (as originally reported in Dimitriadis et al. 2017b, see Table 2).

The second category includes SBNs with edges weighted by the NS, FA, and MD with various combinations of applying absolute thresholding on one individual metric-based SBN while keeping the same sparsity as the 9m-OMST that showed the highest reproducibility (Messaritaki et al., 2019). After the thresholding step, the topology was either kept as it was or re-weighted with one of the remaining two metrics (see Table 2).

C) NS-thr: Keep the highest-NS edges.

D) NS-t/FA-w: Threshold to keep the highest-NS edges, then reweight those edges with their FA.

E) NS-t/MD-w: Keep the highest-NS edges, then reweight those edges with their MD.

In previous studies, we ranked twenty-one graph construction schemes with similarities ranging from 0.99 to 0.42 (Messaritaki et al., 2019) (Table 3). We also focused on the repeatability of graph partitions (Dimitriadis et al., 2021), focusing on

the first five graph construction schemes with the highest topological similarity (Table 2). Fig.1A illustrates the five SBNs from the first scan of the first subject.

Table 2. Summary of the graph-construction schemes

Abbreviation	**Initial Edge Weights**	**Topology**	**Final Edge Weights**	**Symbol**
NS – OMST	NS	OMST	Unchanged	A
9-m OMST	lin. comb. of all 9 metrics in Table 1	OMST	Unchanged	B
NS-thr	NS	keep highest-NS edges	Unchanged	C
NS-t/FA-w	NS	keep highest-NS edges	re-weight with FA	D
NS-t/MD-w	NS	keep highest-NS edges	re-weight with MD	E

2.4 Laplacian Spectrum

2.4.1 The normalized Laplacian matrix

In this paper, we considered the transformation of individual integrated SBNs from the five graph construction schemes to the normalized Laplacian matrix L. The Laplacian matrix L has the advantage that its eigenvalues range between 0 and 2, enabling the direct comparison of SBN across modalities, subjects, cohorts, and of different sizes (Chung, 1996).

The normalized Laplacian matrix is defined as:

$$nL(u,v) = \left\{ \begin{array}{ll} 1, & if\ u = v\ and\ degG(v_i) = 0 \\ -\dfrac{1}{degu}, & if\ u\ and\ v\ are\ connected \\ 0, & otherwise \end{array} \right\} \quad (1)$$

with u and v representing two nodes of the network or brain regions, L(u,v) the edge from node u to v and degu the degree of node u which is the total number of its connections. Fig.1 illustrates the preprocessing steps needed from the original SBN up to the estimation of the normalized Laplacian spectrum given by the normalized Laplacian eigenvalues. Rows correspond to the preprocessing steps of extracting the normalized Laplacian eigenvalues from SBN while columns refer to the five graph construction schemes.

The normalized Laplacian matrix can be also estimated and expressed from its relation with the adjacency matrix A as nL = D^(-1/2)*L*D^(-1/2) (Fig.1D) where the D is the degree matrix, where its diagonal elements encapsulate the degree of every node (Fig.1B), L = D - A is the unnormalized Laplacian matrix (Fig.1C), and A is the adjacency matrix. The eigenanalysis of the nL extracts a collection of eigenvalues λ for which a non-zero vector eigenvector v exists that satisfies the equation $Lv = \lambda v$.

Eigenvalues share important properties. The multiplicity of the eigenvalues equal to 0 (λ = 0) is equal to the number of connected modules (Chung, 1996). The largest

eigenvalue is equal to or smaller than 2, sorting the range of eigenvalues as $0 \leq \lambda 1 \leq \ldots \leq \lambda n \leq 2$ ((Chung, 1996) ; Fig.1E).

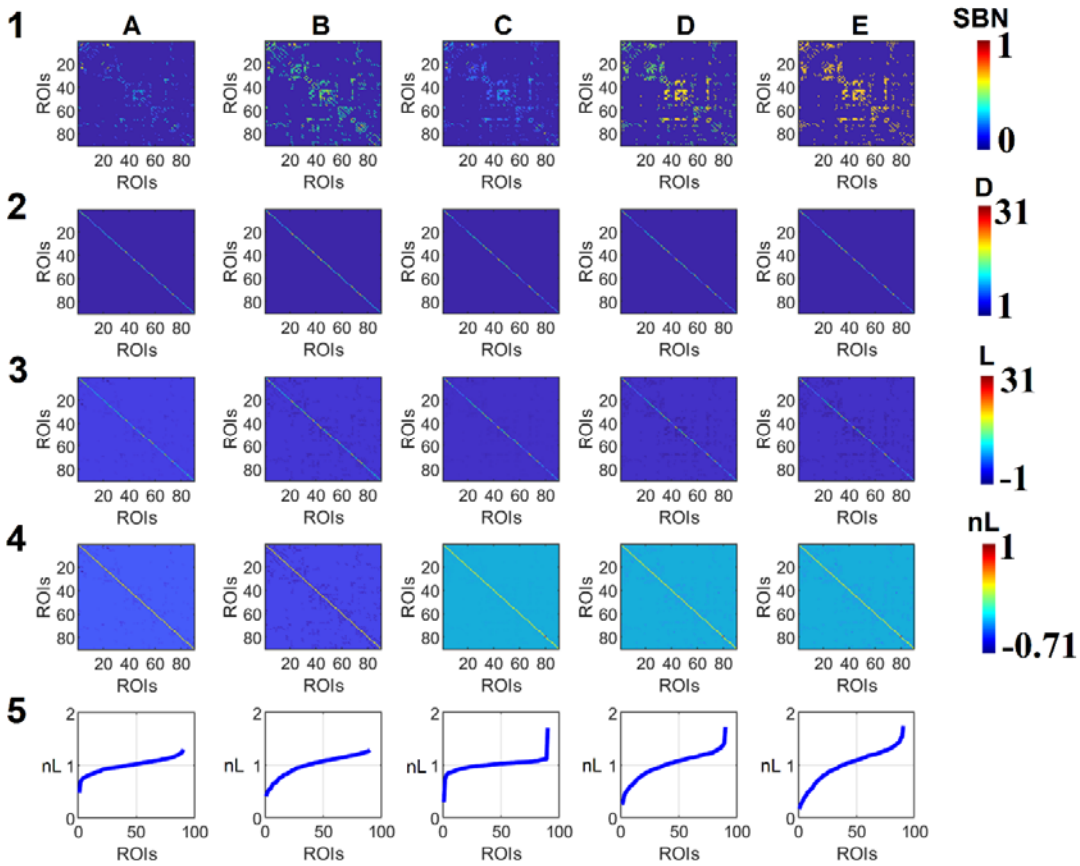

Fig.1 Illustration of preprocessing steps for the estimation of normalized Laplacian eigenvalues. The data are derived from the first scan of the first subject from the dMRI cohort. A-E in columns refer to the five graph construction schemes tabulated in Table 2. Numbers refer to the preprocessing steps:

1. Original metric-based SBN for the five graph construction schemes as they are reported in Table 2.
2. The D degree matrices of the five SBN shown in A
3. The unnormalized Laplacian matrix L of the five SBN
4. The normalized Laplacian matrices nL of the five SBN
5. The normalized Laplacian eigenvalues (nL) linked to the five SBN

2.4.2 Important nL-based properties

Network synchronizability of a variety of complex networks can be characterized by the ratio of the second smallest eigenvalue λ_2 to the largest eigenvalue of the Laplacian matrix λn (Barahona and Pecora, 2002). The following formula (2)

$$LE(G) = \sum_{i=1}^{n} [nL_i \ - 2m/n] \qquad (2)$$

is called the Laplacian energy of the network G, where nL are the normalized Laplacian eigenvalues, m is the number of edges and n is the number of vertices (Hakimi-Nezhaad and Ashrafi, 2014).

2.4.3 Repeatability of Laplacian Eigenvalues, Eigenvectors, and the related properties

We assessed the repeatability of Laplacian eigenvalues per graph construction scheme between the two scans by measuring their Pearson's correlation coefficient (Pcc) (within-session and graph construction scheme). Additionally, Pcc was estimated between Laplacian eigenvalues between graph construction schemes from the same or different scan sessions to further enhance the link between the graph construction scheme and its Laplacian spectrum (between-session and graph construction scheme). We estimated the repeatability of Laplacian eigenvectors (connectome harmonics) per graph construction scheme between the two scans by adopting the signum function (D^{LS}).

$$D^{LS} = \sum_{i=1}^{no\ of\ ROIs} \left| \frac{\sum_{j=1}^{no\ of\ ROIs} sign(LEigenvector_{scan\ 1}^{ij} - LEigenvector_{scan\ 2}^{ij})}{no\ of\ ROIs} \right| \quad (3)$$

where no of ROIs denotes the number of brain areas while the first sum runs across Laplacian eigenvectors and the second sum across its vector size that equals the no of ROIs.

The repeatability of the Synchronizability and Laplacian energy per graph construction scheme and between the two scans was quantified with the absolute difference between the two scans.

2.4.4 Laplacian Spectrum Properties

Many important dynamical network models can be formulated as a linear dynamical system which can be expressed by the following diffusion equation

$$\frac{dc}{dt} = -aLc \ (4)$$

which is a continuous time version.

As we mentioned before, the Laplacian matrix of a network is expressed as L = D – A. The Laplacian matrix is symmetric in which diagonal components are all non-negative (representing node degrees) while the other components are all non-positive.

A ***Laplacian matrix*** of an undirected network has the following interesting properties:

1. At least one of its eigenvalues is zero.
2. All the other eigenvalues are either zero or positive.
3. The number of its zero eigenvalues corresponds to the number of connected components in the network.
4. If the network is connected, the dominant eigenvector is a homogeneity vector $h=(11...1)^T$.
5. The smallest non-zero eigenvalue is called the *spectral gap* of the network, which determines how quickly the diffusion takes place on the network.

Smaller Eigenvalues

Laplacian eigenvalues and the relevant eigenvectors play an important role on the studying of multiple aspects of complex network structures like resistance distance, spanning trees and community structures (Newman,2006). According to Newman's study, only the eigenvectors related to positive eigenvalues could contribute to the partitioning of the network and to the modularity. This practically means that the optimal graph partitioning could be achieved by selecting the number of communities/groups in a network to be equal with the number of positive eigenvalues plus 1. In the normalized Laplacian graph, the important role of guiding the spectral clustering of the network is supported by the smallest normalized Laplacian eigenvalues. The k eigenvectors that correspond to the k smallest eigenvalues of the normalized Laplacian graph create a n x k matrix (where the n refers to vertices of the graph and k to the eigenvectors). Performing a k-Means clustering on the n vertices in the k-dimensional Euclidean space, one can reveal the communities of the graph. Based on the aforementioned properties, the smallest eigenvalues of the Laplacian spectrum reflect the modular organization of a network (Donetti, 2005; Fortunato, 2010; Shen and Cheng, 2010; Shi and Malik, 2000).

The spectral gap is the smallest non-zero eigenvalue of L, which corresponds to the largest non-zero eigenvalue of $-\alpha L$ and thus to the mode of the network state that shows the slowest exponential decay over time. The spectral gap's value determines how quickly the diffusion takes place on the network. If the spectral gap is close to zero, this decay takes a very long time, resulting in slow diffusion. If the spectral gap is far above zero, the decay occurs quickly, and so does the diffusion. The larger the value of the first nonzero eigenvalue of *L* the faster the convergence of the diffusive process. In that sense, the spectral gap of the Laplacian matrix captures some topological aspects of the network, i.e., how well the nodes are connected to each other from a dynamical viewpoint. The spectral gap of a connected graph (or, the second smallest eigenvalue of a Laplacian matrix in general) is called the *algebraic connectivity* of a network.

Every eigenvector v_i informs us of a unique bisection of the nodes of a network assigning to each one a positive or negative value and the associated eigenvalues λ_i express the inverse diffusion time of this dichotomy to the stationary state. Smaller eigenvalues are indicative of longer diffusion times, revealing a larger proportion of inter-module connections and a smaller number of inter-module connections.

The λ_2 eigenvalue provides the possible best division of nodes into two modules and it is called Fiedler value while the corresponding eigenvector is called Fiedler vector (Chung, 1996). One option that is proposed in the literature is the combination of divisions derived from all eigenvectors up to v_i to assign every node to i communities. A possible optimal number of communities can be defined by the largest eigen-difference (eigen-gap) between consecutive Laplacian eigenvalues ($\lambda_{i+1} - \lambda_i$) (Cheng and Shen, 2010; Shi and Malik, 2000). In summary, small eigenvalues, their number, and the eigen-differences reflect important attributes of the modular structure of a network (Fig.2A).

In the present study, we compared the methods of eigen-gap Laplacian differences with the k-means clustering applied over the k eigenvectors that correspond to the k smallest eigenvalues of the normalized Laplacian graph. The second approach creates a n x k matrix (where the n refers to vertices of the graph and k to the eigenvectors). The total sum of the normalized Laplacian eigenvalues in our study equals to 90. We defined the smallest eigenvalues, the first ones where their sum divided by the total sum overcomes the 10%. We ran the k-Means clustering 50 times on the n vertices in the k-dimensional Euclidean space and we

integrated the findings to avoid the influence of the random initializations of the k-Means algorithm. We adopted mutual information MI as in our previous study (Dimitriadis et al., 2021) to measure the similarity of graph partitions per subject and graph construction scheme between the two scans. The outcome of graph partitions affiliations with both the methods is compared with the outcome of the best partition observed in our exploratory analysis with a high number of graph partition algorithms applied in the same dataset (Dimitriadis et al., 2021).

Medium Eigenvalues

Network motifs are statistically significant recurrent subgraphs. All networks like brain networks, biological, social and technological networks can be represented as graphs, which include a large variety of subgraphs. Practically, network motifs are repeatable sub-graphs that are defined by a specific pattern of interactions between vertices. They may also reflect a framework supporting particular functions to achieved in an efficient way (Sporns, and Kötter, 2004). For that reason, the motifs are of high importance to reveal the structural principles of complex networks reflecting their functional properties (Fig.2B). Motifs are characterized by their size that equals the number of vertices and by the repertoire of possible alternative ways that nodes are connected. By defining the number of the studying vertices M, we enumerate exhaustively the frequency of every single motif of size M across its structural connectivity variance. The outcome of this procedure gives the motif frequency spectra for structural motifs of size M. Usually, the size M is restricted within the range of [3 - 5] due to the computational power needed to enumerate exhaustively the motif frequency spectra of a network with a large number of vertices e.g. a few hundreds. Fig.3.A illustrates the repertoire of 2,3,4 motifs for an undirected graph.

It is well studied that repeated duplications and additions of nodes and motifs in the construction of a network leave traces in the network's Laplacian spectrum (Banerjee and Jost, 2009, 2008). In a network, for example, two nodes with a similar connectivity pattern will increase the eigenvalue $\lambda=1$ of the spectrum (Banerjee and Jost, 2008). Duplication of edge motifs, for example, duplication of two connected nodes n_1 and n_2 has been shown to produce symmetrical eigenvalues around 1 with

Laplacian eigenvalues $\lambda_{\pm} = 1 \pm (\frac{1}{\sqrt{d_{n1}d_{n2}}})$, with d_n being the degree of node n. To better understand the relationship between motifs and eigenvalues, we give the following examples. An inclusion of a new triangle motif to a network results in the addition of an eigenvalues λ = 1.5 to the spectrum (Banerjee and Jost, 2008a). The joining or duplication of a motif in a network produces specific eigenvalues in the spectrum and repetition of these processes result in characteristic aggregated eigenvalues observed as peaks of the Laplacian spectrum. For that reason, the eigenvalues with high multiplicities e.g. high peak at λ = 1 or eigenvalues at equal distances around 1 are indicative of a local organization as a consequence of the presence of recursive motifs in the network (Fig.2B).

In the present study, we exhaustively quantified the 3,4 motifs across subjects, scans, and in the five graph construction schemes (Fig.3A). We quantified the total number of 3,4 motifs in the network and also the motif frequency of occurrence around an individual node which is known as the motif fingerprint of that node. To reveal a link between the peak(s) of the Laplacian spectrum and the total number of 3,4 motifs, we adopted a multi-linear regression analysis per graph construction scheme between the total amount of every possible 3 or 4 motif with the relative frequency (RF) linked to peak at λ = 1.

Largest Eigenvalues

The largest eigenvalue of the Laplacian spectrum informs us of the level of 'bipartiteness' of the most bipartite subpart of the network, which is closely related to the number of odd cyclic motifs in the network. A subnetwork is fully bipartite when its nodes can be divided into two groups where nodes of the same group are not connected.

A graph G = (V;E) is bipartite if the vertex set V can be partitioned into two sets A and B (the bipartition) such that no edge in E has both endpoints in the same set of the bipartition. A matching $M \subseteq E$ is a collection of edges such that every vertex of V is incident to at most one edge of M. If a vertex v has no edge of M incident to it then v is said to be exposed (or unmatched). A matching is perfect if no vertex is exposed; in other words, a matching is perfect if its cardinality is equal to $|A| = |B|$. Fig.3C illustrates an example of perfect matchings and exposed edges.

The ‘bipartiteness’ is directly linked to the total number of odd cycle motifs in a network (Fig.2C & Fig.3D). Here, we also estimate the bipartitenes of the SBN with the following bipartivity index b_s (Estrada, 2022)

$$b_s = \frac{trace(\exp(-SBN))}{trace(\exp(SBN))} \quad (5)$$

The bipartivity index b_s equals to 1 for a complete bipartite network while it changes monotonically with the increase of the number of edges “frustrating” the bipartition. The edges that if removed the network becomes bipartite are called frustrated. Such frustrated edges are shown in Fig.3B.

A motif H can be decomposed into a set of disjoint small cycles and stars and this decomposition is valid if all vertices of a motif H belong to either a star or an odd cycle in the set (Fig.3D). A star is a subnetwork type where only a central node is connected with the rest of the nodes while an odd cycle is a subnetwork with an odd number of vertices that are connected between each other in a circular way (Fig.3D). The degree of every node in an odd cycle is 2.

In the present study, we explored the link between the largest eigenvalue and the bipartivity index b_s with the total number of 3-node odd cycles which is the triangle 3-motif presented in Fig.3A. For this purpose, we adopted Pearson’s correlation coefficient applied across the five graph construction schemes.

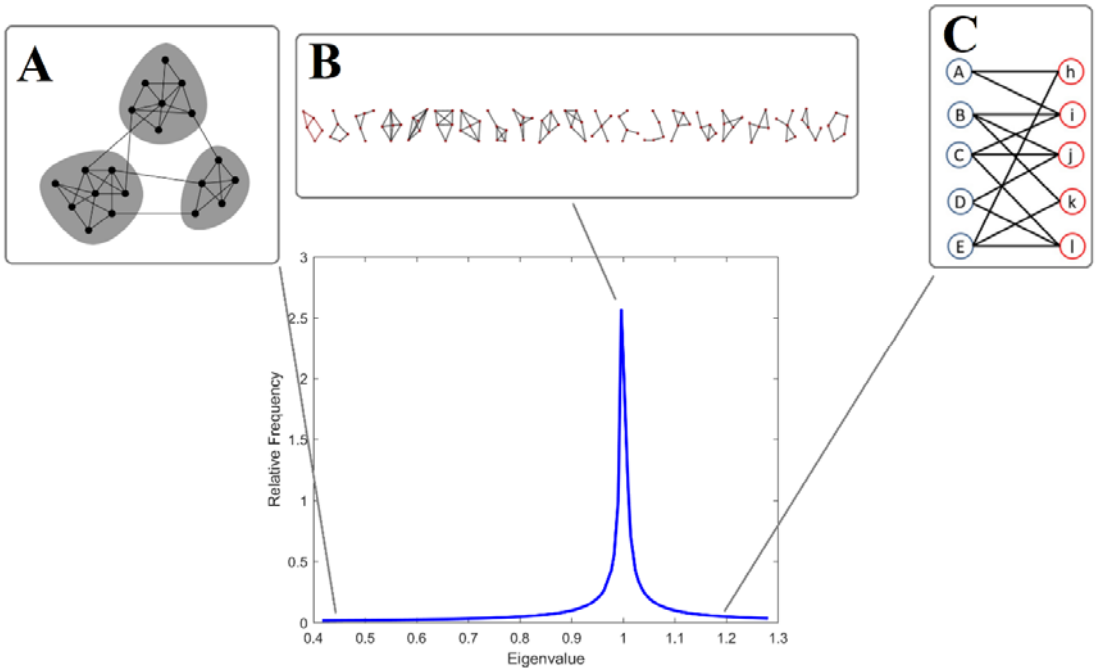

Fig.2 Topological properties of a network reflected in the Laplacian Spectrum

(A) The first smaller Laplacian eigenvalues are indicative of stronger community structures

(B) Recursive motifs in the complex network result in Laplacian eigenvalues of high multiplicities, revealing characteristic peaks in the Laplacian spectrum (λ=1)

(C) The largest eigenvalue reflects the level of 'bipartiteness' of the most bipartite subgraph of the network which is alternatively linked to the total number of odd cyclic motifs of the network.

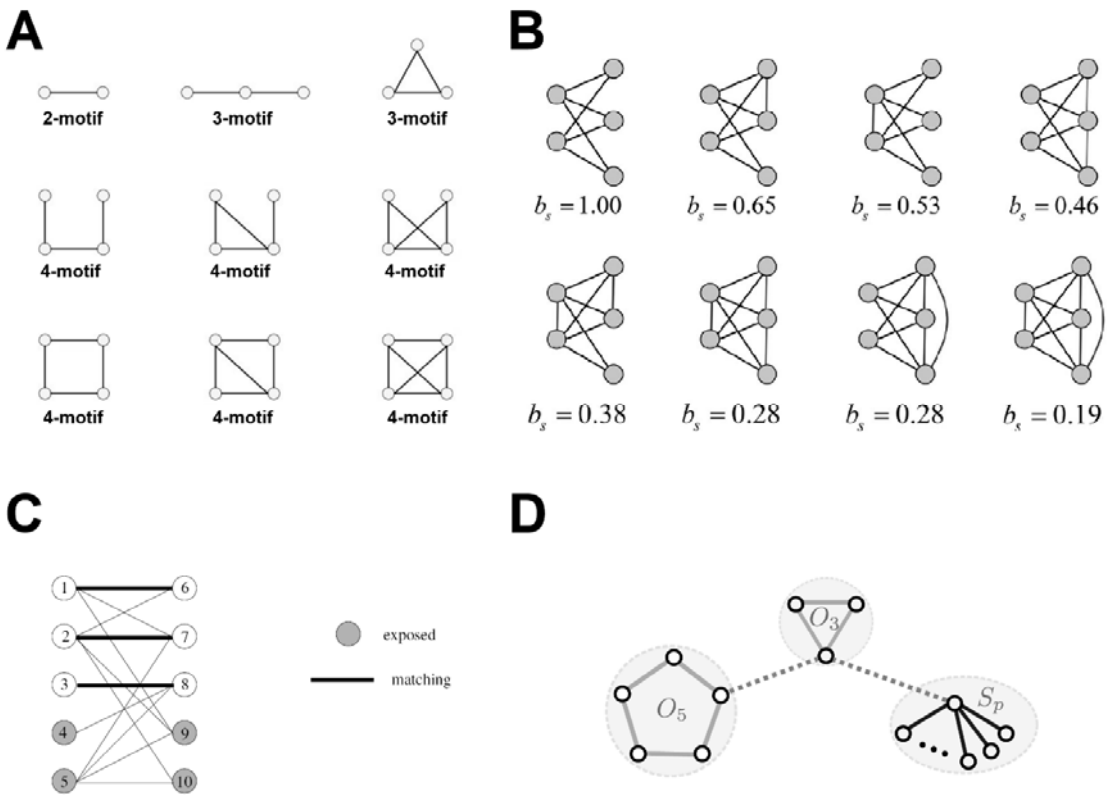

Fig.3. Motifs, bipartivitiy, odd cycles, and stars.

(A) The repertoire of 2-3-4 motifs in an undirected graph

(B) Illustration of the monotonically change in the bipartivity index with the increase in the number of 'frustrated' edges in a complete bipartite graph

(C) The edges (1 - 6), (2 - 7) and (3 - 8) form a matching. Vertices 4, 5, 9 and 10 are exposed.

(D) An example of an optimal decomposition of a motif *H* into odd cycles and stars.

2.4.5 Laplacian Spectrum

We further processes the Laplacian spectrum not as the collection of the eigenvalues λ_j , but their convolution with a smoothing kernel, here a Gaussian, described by the following formula

$$f(x) = \sum_{\lambda_j} \frac{1}{\sqrt{2\pi\sigma^2}} \exp\left(-\frac{|x-\lambda_j|^2}{2\sigma^2}\right) \qquad (6)$$

The particular smoothing value σ was set to 0.015. A discrete smoothed spectrum was used in which f had steps of 0.001. Furthermore, the distribution was normalized such that the total eigenvalue frequency was one.

2.5 Brain Fingerprinting

Another aim of our study was to investigate the repeatability of the Laplacian spectrum of SBN across alternative graph construction schemes. Complementary to the repeatability of Laplacian eigenvalues, we performed an identification analysis across pairs of scans where the second scan consists of the 'target' session and the first scan the 'database' session (Fig.4). Iteratively, one individual's Laplacian eigenvalue was selected from the target set and compared against the N subject-specific Laplacian eigenvalues profile in the database set to find the Laplacian profile that was maximally similar. As a proper dissimilarity distance, we adopted the X^2 statistics (Rubner, 2000). The final outcome of this process is an identity matrix with 1s if the identity had been predicted correctly and 0s if it did not. Finally, we summed up the total number of corrected identifications per graph construction scheme and further divided by the total number of subjects to express the accuracy (performance) of the whole brain fingerprinting process. For a comparison purpose, we investigated the performance in terms of brain fingerprinting of the structural properties of SBN across alternative graph construction schemes separately for communities, 3,4-motifs, bipartiteness , and the total number of odd cycle motifs and also in an ensemble way. We adopted proper metrics for every structural property such as normalized mutual information for the communities, the X^2 statistics for the 3,4-motifs, the Euclidean distance for the bipartiteness and the X^2 statistics for the total number of odd cycle motifs.

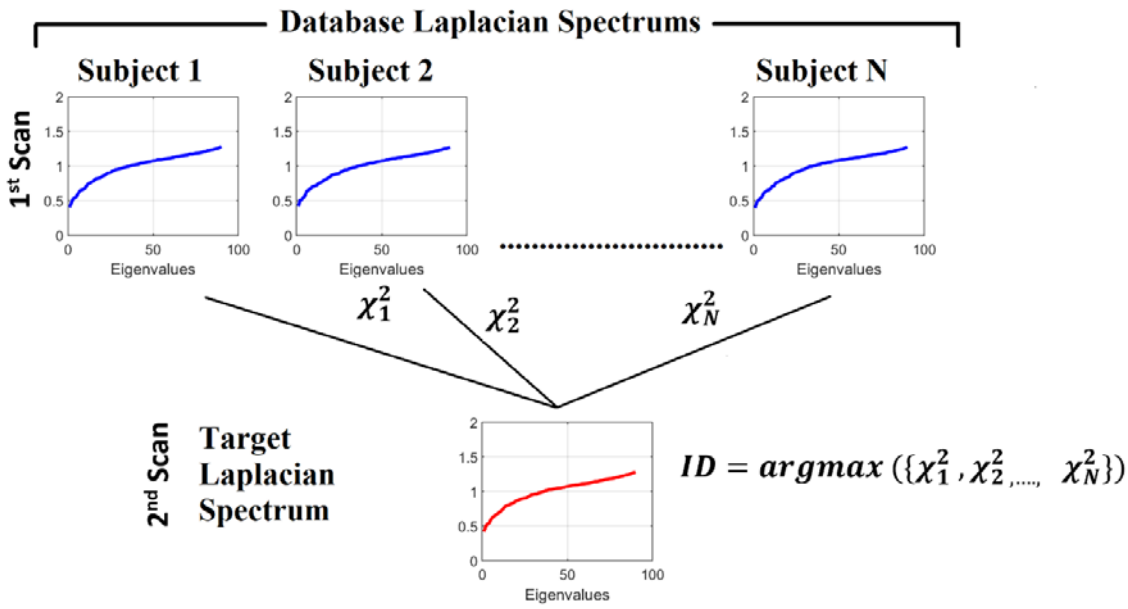

Fig.4 Identification analysis procedure

Identification procedure. Given a query Laplacian eigenvalue profile from the target set, we estimated the Chi-square histogram distance between this Laplacian eigenvalue profile and all the Laplacian eigenvalue profiles in the database. The predicted identity ID* is the one with the highest Chi-square histogram distance value (argmax).

2.6 Statistical Analysis

Below, we describe the statistical analysis followed in our study.

Robustness

To investigate the effect of adding small topological 'noise' to the structural brain networks to the Laplacian spectrum, we randomly rewired 5% of the edges while maintaining the degree and the strength of every node (Maslov and Sneppen, 2002). Ten thousand surrogate null network models were generated per subject, scan, and graph construction scheme. The following measurements were tested between the

original estimates and the surrogates based counterparts for every graph construction scheme.

i) Group-mean λ_2 , group-mean number of communities based on eigen-difference and k-Means clustering over the first eigenvectors across subjects

ii) The MI between the communities extracted with eigen-difference and k-Means clustering from the two scans per graph construction schemes

iii) Group-mean relative frequency (RF) linked to peak around one

iv) Group-mean large eigenvalue λ_n

v) Group-mean total number of the triangle 3-motif

vi) Group-mean bipartivity index bs

vii) Group-mean between scan D^{LS} of the Laplacian eigenvectors

We applied a Wilcoxon Rank-Sum test between the original estimates with the ten thousand surrogate counterparts.

Repeatability of Laplacian Eigenvalues and the Relevant Properties

We quantified the repeatability of Laplacian eigenvalues using Pearson's correlation coefficient (Pcc) accompanied by the relevant p-value. The Pcc was estimated between Laplacian eigenvalues derived from the two scan-sessions from the same graph construction scheme (within-session and graph construction scheme) and also between graph construction schemes from the same or different scan session (between-session and graph construction scheme). We then estimated first per subject and then across the cohort, the group-mean Pcc related to within-session and graph construction scheme and the group-mean Pcc linked to within-session and graph construction scheme. Adopting a Wilcoxon Rank-Sum test, we estimated the significance level between the two Pcc values that will support at which degree the Laplacian eigenvalues are highly dependent on the graph construction scheme.

We also applied the Wilcoxon Rank-Sum test between λ_2, λ_n, and the eigen-difference of the original estimates and the ones derived from the surrogate null models per graph construction scheme and scan sessions.

Repeatability of Laplacian Eigenvectors

We first applied a Wilcoxon Rank-Sum test between the original D^{LS} values with the surrogate D_{surr}^{LS} values per graph construction scheme. We then adopted a Wilcoxon Rank-Sum test applied to every pair of D^{LS} values dedicated to graph construction schemes.

Multiple Comparison Correction

We applied the false discovery rate (q = 0.01) to correct for multiple comparisons.

3. Results

3.1 High Repeatability of Laplacian Eigenvalues

Laplacian eigenvalues were highly repeatable across the five graph construction schemes (within-session and graph construction scheme; Pcc = 0.99 +- 0.01, p-value = 0.014×10^{-16} +-0.0009×10^{-16}). The between-session and graph construction scheme correlation was Pcc = 0.89+-0.10, p-value = 0.013×10^{-16} +- 0.0011×10^{-16}. The Wilcoxon Rank-Sum test revealed a strong difference in Pcc values compared to the within-session and graph construction scheme and between-session and graph construction scheme (p-value = 0.0021). Fig.5 illustrates the Pcc values between all the combinations across the five graph construction of the schemes and scan sessions for subject 1.

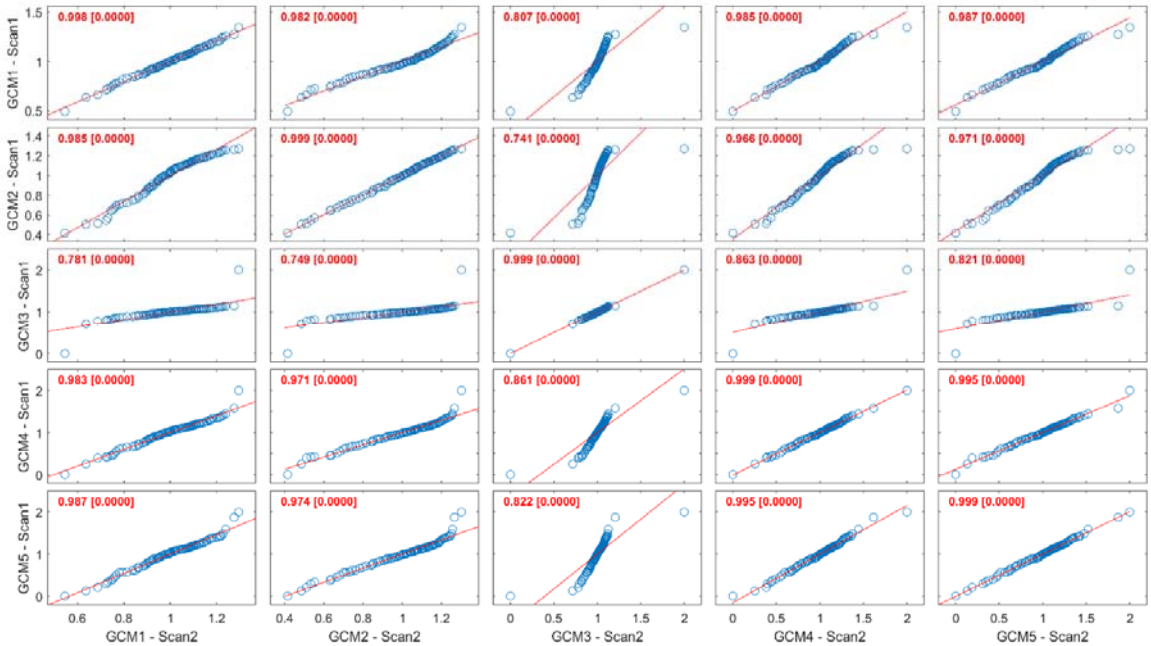

Fig.5 Pcc values between all the combinations across the graph construction schemes and scan sessions for subject 1. The main diagonal reports the repeatability estimations of the Laplacian eigenvalues (within-session and graph construction scheme) while the off-diagonal refers to the between-session and graph construction schemes.

3.2 Repeatability of the Laplacian Eigenvalue Properties

Fig.6 summarizes the group-mean and absolute between-scan differences of the Synchronizability and the Laplacian Energy for every graph construction scheme. Interestingly, the range of Synchronizability shows a higher dependency on the graph construction scheme compared to the Laplacian energy. Our observations are supported by a direct comparison of original values with the surrogate-based Laplacian properties as shown in the following brackets. The smallest group-mean between-scan difference for Synchronizability is shown for the 9m-OMST (p-value = 0.0041) and NS-OMST (p-value = 0.0021) graph construction schemes and the Laplacian energy is shown for 9m-OMST (p-value = 0.0032) and NS – OMST (p-value = 0.0022) graph construction schemes.

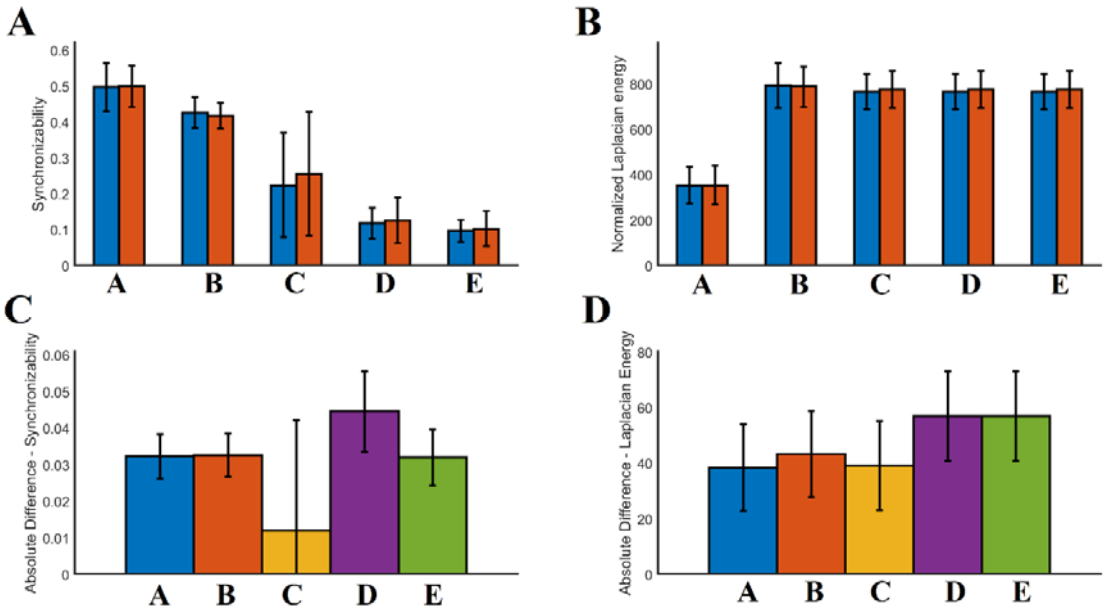

Fig.6 illustrates the group-mean Synchronizability and Laplacian Energy for every graph construction scheme.

A. Group-mean Synchronizability, B. group-mean Laplacian Energy, Group-mean between-scan absolute difference for C. the Synchronizability and D. the Laplacian Energy properties. (Letters from A to E refer to the five graph construction schemes defined in Table 2). In A and B, blue/red colors refer to the first and second scan sessions, correspondingly.

3.3 Laplacian Sub-spectrum findings

Smaller Eigenvalues

Table 3 summarizes the group-mean λ_2, the number of modules revealed by the eigen-difference of Laplacian eigenvalues and by the k-Means clustering applied over the first eigenvectors. For the first two graph construction schemes (NS-OMST, 9m-OMST) compared to the surrogate null models, the average λ_2 revealed that the original SBN can be subdivided in two subnetworks, while the eigengap and the k-Means approaches for the detection of communities showed significant difference findings ($p < 0.001$). The number of communities as detected with k-Means for the 9m-OMST graph construction scheme is much closer to our best findings (Dimitriadis et al., 2021).Table 4 tabulates the MI of between-scan communities affiliations

extracted with both methods and in every graph construction scheme. For the first two graph construction schemes (NS-OMST, 9m-OMST), the MI values for the k-Means algorithm are high, while the statistical comparison of the MI between the k-Means and the eigengap algorithms ($p < 0.001$) untangled the k-Means algorithm as a better approach compared to the eigengap. The communities extracted with k-Means with the 9m-OMST method showed a high similarity with our previous study ($MI = 0.93 \pm 0.05$) where numerous graph partition algorithms were applied on the same set (Dimitriadis et al., 2021).

Table 3. Group-mean λ_2 , the number of communities based on eigen-difference and k-Means clustering over the first eigenvectors across subjects for every graph construction scheme. We underlined with bold, the p-values that showed significant differences compared to the surrogate-based p-values (Letters from A to E refer to the five graph construction schemes defined in Table 2.

	A	**B**	**C**	**D**	**E**
λ_2(mean+/-std)	0.65±0.06	0.62±0.04	0.42±0.24	0.22±0.06	0.18±0.05
λ_2^{surr}(mean +/-std)	0.42±0.05 (**p = 0.0012**)	0.43±0.05 (**p = 0.0034**)	0.38±0.17 (p = 0.062)	0.20±0.05 (p = 0.059)	0.17±0.04 (p = 0.071)
Eigengap(mean+/-std)	2.4±0.2	3.3±0.6	2.9±0.7	2.2±0.6	2.1±0.2
Eigengap^{surr}(mean+/-std)	1.5±0.4 **(p = 0.0037)**	2.2±0.5 **(p = 0.0056)**	2.1±0.6 (p = 0.069)	2.0±0.7 (p = 0.07)	1.5±0.3 (p = 0.061)

k-Means(mean+/-std)	7.2±1.2	8.8±0.4	4.2±1.2	2.9±1.2	2.8±0.8
k-Means^{surr}(mean+/-std)	3.2±1.3 **(p = 0.0024)**	4.1±1.3 **(p = 0.0042)**	3.9±1.1 (p = 0.693)	2.0±1.6 (p = 0.736)	1.6±0.5 (p = 0.615)

Table 4. The MI between the communities extracted with eigen-difference and k-Means clustering from the two scans per graph construction schemes. We underlined with bold, the p-values that showed significant differences compared to the surrogate-based p-values (Letters from A to E refer to the five graph construction schemes defined in Table 2.

	A	**B**	**C**	**D**	**E**
k-Means(mean+/-std)	0.79±0.06	0.89±0.04	0.45±0.12	0.22±0.11	0.39±0.12
k-Means^{surr} (mean+/-std)	0.36±0.05 (**p = 0.12x10^{-15}**)	0.47±0.08 (**p = 0.0034**)	0.33±0.17 (p = 0.627)	0.20±0.07 (p = 0.592)	0.23±0.14 (p = 0.071)
Eigengap(mean+/-std)	2.4±0.2	3.3±0.6	2.9±0.7	2.2±0.6	2.1±0.4
Eigengap^{surr}(mean+/-std)	1.5±0.4 **(p = 0.0037)**	2.2±0.5 **(p = 0.0056)**	2.1±0.6 (p = 0.374)	2.0±0.7 (p = 0.538)	1.6±0.3 (p = 0.418)

Medium Eigenvalues

The Laplacian spectrum of the graph construction schemes showed a single clear smooth peak as presented in Fig.2. This peak around 1 suggests a number of motif duplications where its height is relevant to this number. The relationship between the relative frequency (RF) linked to peak at λ = 1 and the total number of unique 3 or 4 motifs is described below. The Laplacian spectrum of structural brain networks across subjects, scans, and graph construction schemes didn't show any other clear peaks indicative of recurrent addition of motifs. Our findings are supported by the surrogate analysis where peaks of significant lower amplitude were observed in surrogated Laplacian spectrums. All distributions showed a peak around 1 while the group-mean relative frequency (RF) related to this peak didn't show differences across methods ($p > 0.05$) but showed difference between original and surrogate null models (Table 5).

Table 5. Group-mean relative frequency (RF) linked to peak around one across subjects for every graph construction scheme. We underlined with bold, the p-values that showed significant differences compared to the surrogate-based p-values (Letters from A to E refer to the five graph construction schemes defined in Table 2.

	A	**B**	**C**	**D**	**E**
RF(mean+/-std)	1.88±0.06	2.61±0.05	2.51±0.14	2.57±0.08	2.48±0.12
$\boldsymbol{RF^{surr}}$ **(mean+/-std)**	1.26±0.11 (**p = 0.14x10^{-11}**)	1.67±0.09 (**p = 0.25x10^{-10}**)	1.63±0.15 (p = **0.38x10^{-11}**)	1.59±0.12 (p = **0.62x10^{-11}**)	1.52±0.13 (p = **0.53x10^{-11}**)

The multi-linear regression analysis revealed a significant trend between the RF and the motifs only for the 9m-OMST graph construction scheme. The following equation described the relationship between the RF and the 5th – 6th 4,motifs only (see Fig.3A):

where

Figs 7-8 show the averaged across subjects and scans motif fingerprint of every node (ROI) across the five graph construction schemes and 3,4 motifs repertoire.

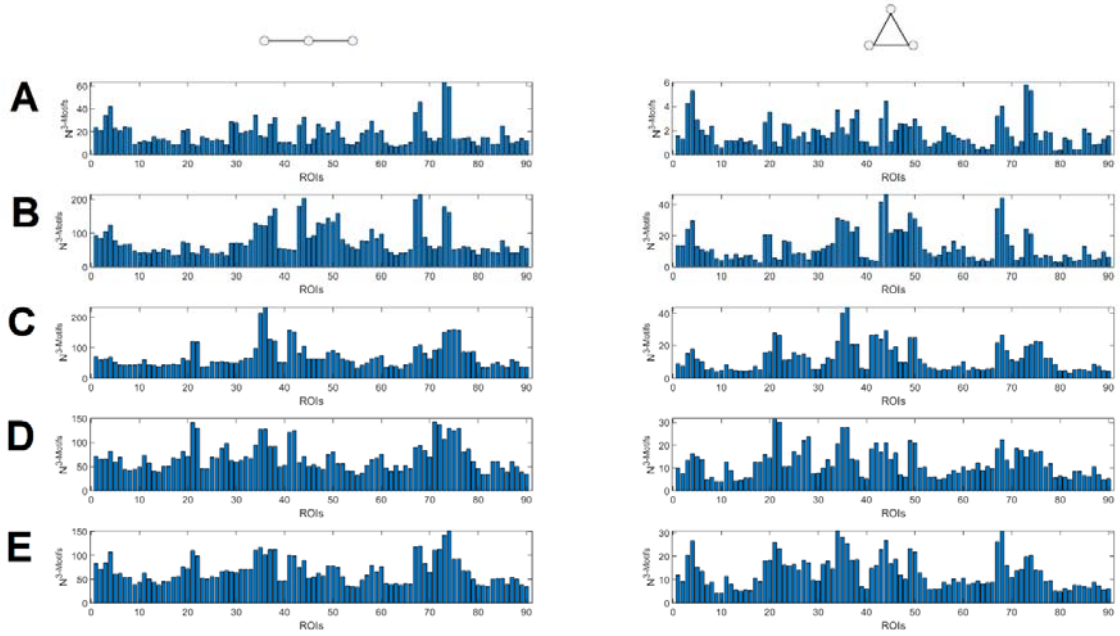

Fig.7. Group and scan averaged motif fingerprint of every ROI across the five graph construction schemes (A-E) and the two 3,motifs.

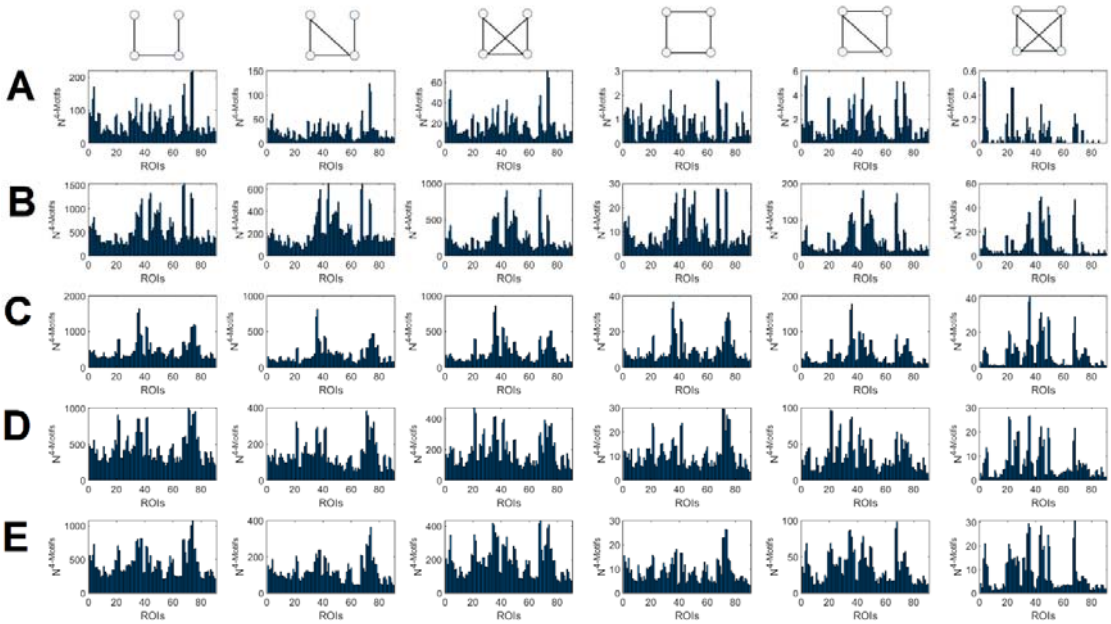

Fig.8. Group and scan averaged motif fingerprint of every ROI across the five graph construction schemes (A-E) and the two 4,motifs.

Largest eigenvalues

Table 6 summarizes the group-mean largest eigenvalue λ_n across graph construction schemes which differs significantly from the largest eigenvalue relevant to the random networks. The largest eigenvalue of the Laplacian spectrum informs us of the level of 'bipartiteness' of the most bipartite subpart of the network, which is closely related to the number of odd cyclic motifs in the network. Visual inspection of the associated eigenvector linked to the largest eigenvalue across the cohort, scans, and in the first two graph construction schemes (NS-OMST, 9m-OMST) with respect to communities as detected in (Dimitriadis et al., 2021) (Fig.5), is highly localized in modules 8 and 9.

Table 7 shows the group-mean 3-motif fingerprint related to the triangle odd-cycle across the graph construction schemes. The 3-motif fingerprint was significantly different for all the graph construction schemes compared to the random networks.

Table 8 tabulates the group-mean bipartivity index b_s across the graph construction schemes. The bipartivity index b_s was significantly different only for the first two graph construction schemes (NS-OMST, 9m-OMST) compared to the random networks. Interestingly, the first graph construction scheme produces the highest bipartivity compared to the rest of graph construction schemes.

Interestingly, the first graph construction scheme showed the highest bipartivity index b_s and the lower number of odd-cycles as presented with the triangle 3-motif showed in Fig.3A. The Pearson's correlation coefficient between the bipartivity index b_s and the number of odd-cycles across the five graph construction schemes was -0.99±0.02 for the first scan and -0.98±0.01 for the second scan.

In contrast, the Pearson's correlation coefficient between the largest eigenvalue and the number of odd-cycles estimated on the 3-motif level across the five graph construction schemes was 0.19±0.01 for the first scan and 0.20±0.01 for the second scan.

Table 6. Group-mean large eigenvalue λ_n. (Letters from A to E refer to the five graph construction schemes defined in Table 2). **We underlined with bold, the p-values that showed significant differences compared to the surrogate-based p-values** (Letters from A to E refer to the five graph construction schemes defined in Table 2).

	A	**B**	**C**	**D**	**E**
λ_n(mean+/-std)	1.31±0.04	1.29±0.02	1.32±0.02	1.28±0.02	1.29±0.02
λ_n^{surr}(mean +/-std)	1.05±0.06 **(p = 0.34x10^{-13})**	1.05±0.04 **(p = 0.51x10^{-15})**	1.03±0.05 **(p = 0.21x10^{-14})**	1.02±0.06 **(p = 0.37x10^{-12})**	1.04±0.05 **(p = 0.51x10^{-14})**

Table 7. Group-mean total number of the triangle 3-motif. (Letters from A to E refer to the five graph construction schemes defined in Table 2). **We underlined with bold, the p-values that showed significant differences compared to the surrogate-based p-values** (Letters from A to E refer to the five graph construction schemes defined in Table 2).

	A	**B**	**C**	**D**	**E**
$N^{3-motif}$ **(mean+/-std)**	18.32±0.99	79.51±18.13	80.55±16.21	76.54±16.84	67.36±13.67
$N_{surr}^{3-motif}$ **(mean+/-std)**	7.32±1.12 **(p = 0.62x10^{-11})**	32.51±12.57 **(p = 0.42x10^{-13})**	39.83±13.72 **(p = 0.29x10^{-12})**	32.54±14.71 **(p = 0.12x10^{-13})**	39.72±9.72 **(p = 0.82x10^{-15})**

Table 8. Group-mean bipartivity index b_s. (Letters from A to E refer to the five graph construction schemes defined in Table 2). **We underlined with bold, the p-values that showed significant differences compared to the surrogate-based p-values** (Letters from A to E refer to the five graph construction schemes defined in Table 2).

	A	**B**	**C**	**D**	**E**
b_s(mean+/-std)	0.91±0.02	0.18±0.05	0.17±0.07	0.18±0.05	0.20±0.07
b_s^{surr}(mean+/-std)	0.14±0.06 **(p = 0.73x10^{-14})**	0.05±0.04 **(p = 0.81x10^{-15})**	0.08±0.05 **(p = 0.634)**	0.11±0.05 **(p = 0.791)**	0.11±0.05 **(p = 0.735)**

3.4 Repeatability of Laplacian Eigenvectors

Table 9 reports the group-mean between-scan MI of the Laplacian eigenvectors for every graph-construction scheme. 9m-OMST graph construction scheme showed the smallest group-mean D^{LS} followed by the FA-t/NS-w but without reaching the significant level (see Fig.9 ; p-value < 0.05, Bonferroni corrected). Our findings are supported also by the direct comparison of original D^{LS} values with the surrogate D^{LS} values (p-value = 0.0057 & p-value = 0.0043, for 9m-OMST and NS-OMST, correspondingly). An overview of the two Laplacian eigenvectors (connectomic harmonics) from both scan sessions for 9m-OMST are illustrated in Fig.10.

Table 9. Group-mean between scan D^{LS} of the Laplacian eigenvectors for every graph construction scheme. We underlined with bold, the p-values that showed significant differences compared to the surrogate-based p-values (Letters from A to E refer to the five graph construction schemes defined in Table 2).

	A	**B**	**C**	**D**	**E**
D^{LS}(mean+/-std)	7.81±1.32	5.91±1.43	7.45±1.67	6.35±1.41	6.41±1.81
D^{LS}_{surr} (mean+/-std)	5.32±1.51	3.85±1.57	6.89±1.32	5.84±1.57	5.87±1.64
	(p = 0.0043)	**(p = 0.0057)**	(p = 0.079)	(p = 0.081)	(p = 0.072)

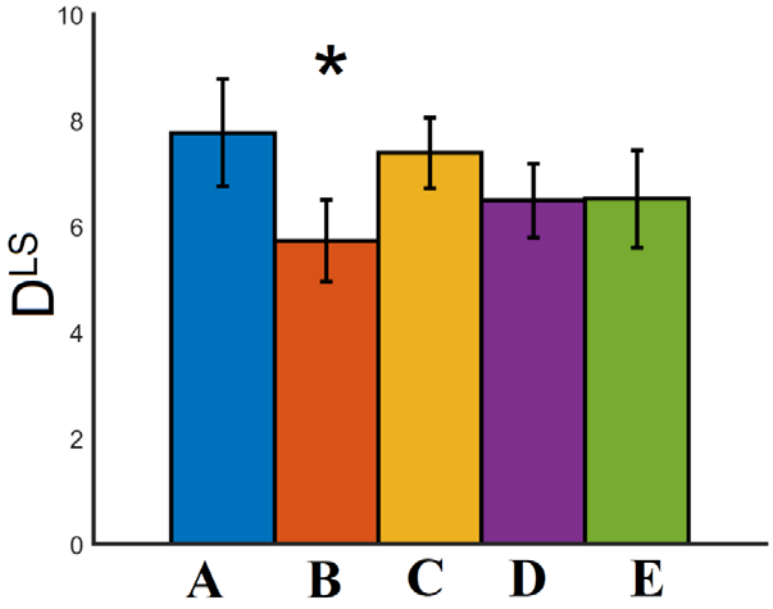

Fig. 9. Illustration of the group-mean D^{LS} for every graph construction scheme. (* denotes the statistical difference of D^{LS} for the 9m-OMST method versus the four methods)

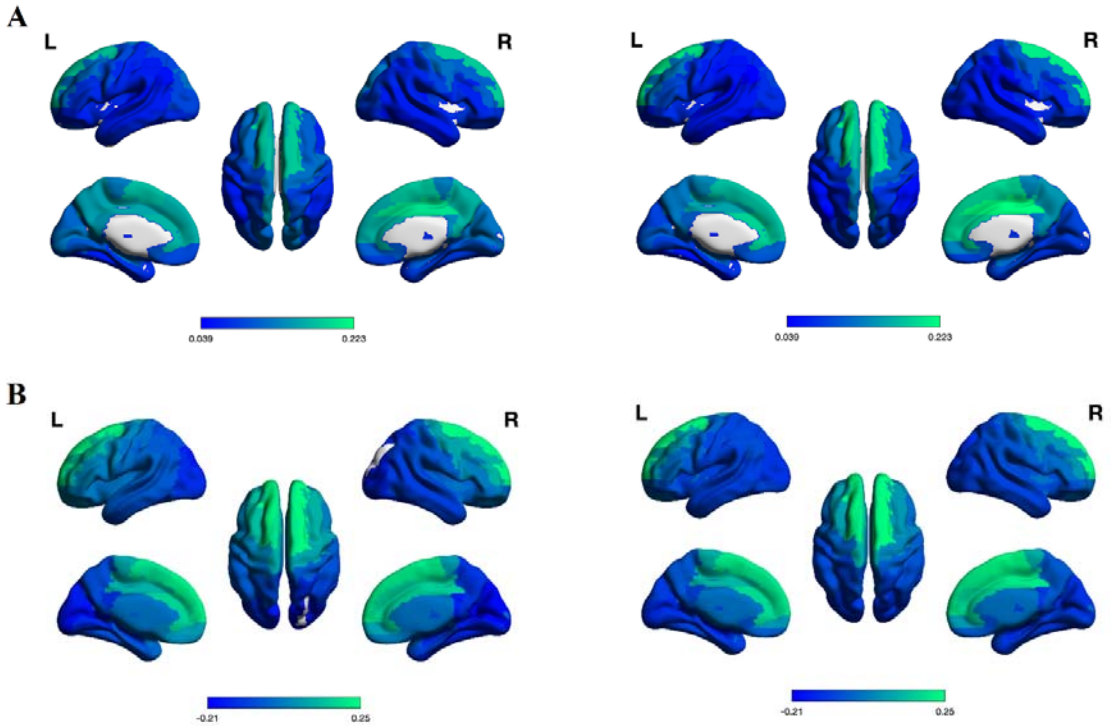

Fig.10. Overview of the two Laplacian eigenvectors (connectomic harmonics) from both scan sessions for 9m-OMST method extracted from subject 1.

A. First eigenvector from scan 1 (left) and scan 2 (right)
B. Second eigenvector from scan 1 (left) and scan 2 (right)

3.5 Brain Fingerprinting

Our analysis succeeded in an accurate identification of subjects id (100%) on the test set (second session) on every graph construction scheme employing the Laplacian spectrum as a feature vector. Complementary, Table 10 shows the Identification accuracy of structural properties of SBN across alternative graph construction schemes. Across the five studying structural properties, the highest

accuracies were detected for communities, and 3,4-motifs across the five construction scheme while the highest performance was detected for 9m-OMST (B), and NS-OMST (A) with the former to get higher accuracies. The combination of the outcome of brain identification strategy for communities, and 3,4-motifs (ensemble way) gave an absolute accuracy (100%) for the 9m-OMST (B) , and a 91.89 for the NS-OMST (A).

Table 10. Identification accuracy of structural properties of SBN across alternative graph construction schemes. (Letters from A to E refer to the five graph construction schemes defined in Table 2).

	A	**B**	**C**	**D**	**E**
Communities	83.78	**89.19**	56.76	59.46	54.05
3-motifs	86.49	**97.30**	71.62	71.62	71.62
4-motifs	89.19	**94.59**	64.86	62.16	67.57
Bipartiveness	45.95	**51.35**	37.84	37.84	40.54
Odd cycle motifs	43.24	**67.57**	40.54	37.84	43.24

4. Discussion

Here, we used test-retest dMRI data from the Human Connectome Project to explore the relation between the spectrum of a graph, i.e., the eigenvalues of its adjacency matrix, and the structure of the graph which is the main goal of spectral graph theory. Under this content, we investigated the repeatability and individuality of the Laplacian eigenvalue spectrum and the Laplacian eigenvectors (connectome harmonics) of the structural brain networks derived from dMRI. Additionally, we explored the repeatability and individuality of the relevant structural properties of the

SBN and also their relationship with the Laplacian spectrum. Finally, we studied how the aforementioned structural network measurements are influenced by the graph construction scheme. For that purpose, we analyzed the test-retest MRI and diffusion-MRI data set from the multimodal neuroimaging database of the Human Connectome Project (HCP) (Glasser et al., 2013; S N Sotiropoulos et al., 2013; Van Essen et al., 2013).

. The main findings of our study are as follows:

1. normalized Laplacian eigenvalues of dMRI-based structural brain networks are subject-specific, and therefore be used to 'fingerprint' an individual, and identify matched connectomes from a pool. Normalized Laplacian eigenvalues are also repeatable across the five graph construction schemes but their connectome-related information of the studying SBN is highly dependent on the graph construction scheme.
2. The combination of the outcome of brain identification strategy for communities, and 3,4-motifs (ensemble way) gave an absolute accuracy (100%) for the 9m-OMST (B) 91.89 for the NS-OMST (A).
3. The repeatability of Laplacian spectrum properties and structural properties of SBN is highly dependent on the graph construction schemes
4. The repeatability of Laplacian sub-spectrum values is also highly dependent on the graph construction schemes
5. K-means algorithm applied over the first Laplacian eigenvectors compared to the eigengap approach applied over the eigen-difference of Laplacian eigenvalues is a better way for detecting graph communities
6. A significant trend was revealed between the RF and the 3,4-motifs only for the 9m-OMST graph construction scheme which was repeatable
7. The bipartivity index b_s showed a negative and repeatable relationship with the number of odd-cycles across the five graph construction schemes
8. The bipartivity index b_s showed a positive and repeatable relationship with the largest eigenvalue across the five graph construction schemes
9. The repeatability of connectome harmonics shows a heavy dependency on the graph construction scheme and lower repeatability compared to Laplacian eigenvalues.

10. Our results provide a proof of concept for repeatable identification of the graph Laplacian spectrum and part of structural properties of SBN based on the selected graph construction scheme.

Investigation of the small eigenvalues from the Laplacian spectrum untangled a community structure for the first two graph construction schemes (NS-OMST, 9m-OMST). For those graph construction schemes, the average λ_2 revealed a high level of community structure while the optimal division of the network based on the eigen-difference is suggested to be between 7 and 9 communities (Dimitriadis et al., 2021). Our findings are supported by the direct comparison with the surrogate null models. In a recent exploratory study on the same dataset comparing thirty-three graph partition schemes and the same set of graph construction schemes, we revealed a consensus set of 9 communities (Dimitriadis et al., 2021; Fig.5). The Laplacian spectrum of the graph construction schemes showed a clear smooth peak as is shown in Fig.3. This peak around 1 suggests a number of motif duplications where its height is relevant to this number. The Laplacian spectrum didn't show any other clear peaks indicative of recurrent addition of motifs. The observation of this peak on the middle subpart of the Laplacian spectrum was consistent across the graph construction schemes while it was less peaked (lower amplitude) in the rewired surrogate networks.

We investigated also the repeatability and the influence of graph construction schemes on basic Laplacian properties apart from the three sub-ranges of Laplacian spectrum. The range of Synchronizability shows a higher dependency on the graph construction scheme compared to the Laplacian energy. The smallest group-mean between-scan difference for Synchronizability is shown for the 9m-OMST and NS-OMST graph construction schemes and for Laplacian energy is shown for 9m-OMST and NS – OMST graph construction schemes. Both observations are supported statistically by a direct comparison with the corresponding values estimated from the surrogate null networks.

The repeatability of Laplacian eigenvectors (connectome harmonics (Naze et al., 2021)) is highly dependent on the graph construction scheme. 9m-OMST graph construction scheme showed the smallest group-mean D^{LS} followed by the NS-OMST but without reaching the significant level ($p < 0.05$, Bonferroni corrected).

These findings are supported also by the direct comparison of original MI values with the surrogate D^{LS} values. However, the group-mean D^{LS} even for the 9m-OMST method is far away from characterized as repeatable.

Our analysis showed that the k-Means clustering applied over the first eigenvectors is a better approach compared to the eigengap approach based on the the eigen-difference of Laplacian eigenvalues. For the first two graph construction schemes (NS-OMST, 9m-OMST), the MI values for the k-Means algorithm are high, while the communities extracted with k-Means with the 9m-OMST method showed a high similarity with our previous study ($MI = 0.93 \pm 0.05$) where a large number of graph partition algorithms were applied on the same set (Dimitriadis et al., 2021).

We explored a possible relationship between the RF extracted from the Laplacian spectrum and the 3,4-motifs extracted from the SBN. Our multilinear analysis untangled a significant trend between the RF and the 3,4-motifs only for the 9m-OMST graph construction scheme which was repeatable. The largest Laplacian eigenvalues reflect the level of bipartiteness of the structural brain networks. Bipartiteness is related to the odd cyclic motifs, and especially is linked to the triangle motifs and high clustering coefficient observed in small-world brain networks (Bassett and Bullmore, 2006; Bullmore and Sporns, 2009; Hagmann et al., 2008; van den Heuvel et al., 2008). In our study, bipartiteness which is expressed with the largest Laplacian eigenvalue Ln was significantly different on the original SBN compared to the surrogate null networks only for the two graph construction schemes (NS-OMST, 9m-OMST). The Pearson's correlation coefficient between the bipartivity index b_s and the number of odd-cycles across the five graph construction schemes was -0.99±0.02 for the first scan and -0.98±0.01 for the second scan. In contrast, the Pearson's correlation coefficient between the largest eigenvalue and the number of odd-cycles estimated on the 3-motif level across the five graph construction schemes was 0.19±0.01 for the first scan and 0.20±0.01 for the second scan.

Under the brain fingerprinting framework, the Laplacian spectrum showed an absolute accuracy (100%). In parallel, the performance in terms of brain fingerprinting of the five studying structural properties revealed the communities, and 3,4-motifs across the five construction scheme succeeding the highest performance for 9m-OMST (B), and NS-OMST (A) with the former to get higher accuracies. The combination of the outcome of brain identification strategy for communities, and 3,4-

motifs (ensemble way) gave an absolute accuracy (100%) for the 9m-OMST (B) , and a 91.89 for the NS-OMST (A).

The spatial resolution of structural brain networks restricted by the adopted anatomical atlas, is likely to have a high impact on the network topology and the relevant Laplacian spectrum (Bullmore and Sporns, 2012, 2009). Our findings can be considered only for reconstructed anatomical brain networks based on dMRI (Hagmann et al., 2008; Iturria-Medina et al., 2008; van den Heuvel and Hulshoff Pol, 2010). The Laplacian Spectrum of functional brain networks using electroencephalography, magnetoencephalography, and functional magnetic resonance imaging (fMRI) might differ from structural brain networks from dMRI. Future studies should reveal the relationship between the Laplacian spectrum of functional and structural brain networks. Recent studies used atlas-free connectome harmonics dMRI as a dependent variable to predict the brain resting-state activity of fMRI (independent variables). They showed their findings in datasets across the landscape of consciousness with very interesting findings (Atasoy et al., 2018a, 2016; Luppi et al., 2020) and in psychedelic (Atasoy et al., 2018b) while they explored the robustness of connectome harmonics using local gray matter and long-range white matter (Naze et al., 2021).

The structural brain networks microscopically showed a community structure as it has been observed in other species and other types of networks (de Lange et al., 2014). Macroscopically, anatomical connectivity topology is shaped by evolutionary growth constraints that attempt to balance the optimal efficiency and robustness of the communication of various brain networks while simultaneously minimizing wiring cost (Bullmore and Sporns, 2012; Collin et al., 2014; van den Heuvel and Sporns, 2013a, 2013b). The 9m - OMST graph construction scheme that integrates nine diffusion metric-based structural brain networks into one has at its core the OMST topological filtering methodology that optimizes efficiency routing via wiring cost (Dimitriadis et al., 2018, 2017b, 2017c, 2017a; Messaritaki et al., 2019).

Here, we demonstrate that the Laplacian spectrum including the Laplacian eigenvalues, eigenvectors, and specific sub-ranges of the Laplacian spectrum are repeatable but only for specific graph constructions schemes. Importantly, the Laplacian eigenvalues are subject-specific while their distribution depends on the size of the network which is the number of brain regions based on the adopted anatomical atlas, its density, and topology (Chung, 1996). It would be very important

to explore the repeatability of the Laplacian spectrum on structural brain networks from dMRI in an atlas-free scenario.

Our study has a few limitations which is important to discuss. Our results were extracted by analysing the HCP dataset, and for that reason it cannot be generalized to other datasets that are acquired with different protocols or scanners or analytic pipelines involving alternative tractography algorithms. It is highly recommended to every researcher to record a percentage of the original cohort across three or more scanning sessions. Moreover, scanning the subjects at the same time of day would be also desirable (Trefler et al., 2016). Many alternative topological filtering schemes have been proposed so far. In our study, we fixed the sparsity of the thresholded networks such as to have the same sparsity as the OMST networks. Other alternative topological filtering schemes with arbitrary or data-driven approach could be also explored under the reproducibility framework. It is important to note here that many other variables can affect the repeatability of structural brain network analyses. There variables include: the parcellation scheme used, the time interval between the test-retest scans, and the resolution of the MR data. There variables should be considered when interpreting structural brain network studies, and a useful discussion of this subject is provided by Welton et al. (2015).

5.Conclusions

In this study, we presented and compared five alternative graph construction schemes for structural brain networks. We then followed a Laplacian spectrum analysis with the main scope to reveal the repeatability of Laplacian eigenvalues, Laplacian eigenvectors, and the related graph properties derived from the Laplacian spectrum. We found a high repeatability of Laplacian eigenvalues, but low repeatability of Laplacian eigenvectors, Laplacian spectrum properties, and of Laplacian sub-spectrum values. We also explored the relationship between structural properties of SBN and the Laplacian spectrum and their feasibility under a brain fingerprinting scenario. Our analysis showed that the Laplacian eigenvalues are also subject-specific and could be used in a brain-fingerprinting scenario across the five graph construction schemes. However, all our findings are highly dependent on the

graph construction scheme, and this should be taken into consideration on the design of any analytic pipeline.

Declarations of interest

None.

Data and code availability

The HCP test-retest data is freely available as listed above. The code used to generate the graphs for the structural brain networks with the OMST schemes is available at: *ttps://github.com/stdimitr/multi-group-analysis-OMST-GDD*. The code used to perform the reproducibility analysis is not freely available, but is based exclusively on Matlab functions. This adheres to the data and code requirements of our funders.

Acknowledgements

We are grateful to the Human Connectome Project for making the test-retest data freely available. The work was partly funded under the BRAIN Biomedical Research Unit, which is funded by the Welsh Government through Health and Care Research Wales. This research was funded in whole, or in part, by a Wellcome Trust Investigator Award (096646/Z/11/Z) and a Wellcome Trust Strategic Award (104943/Z/14/Z). For the purpose of open access, the author has applied a CC BY public copyright licence to any Author Accepted Manuscript version arising from this submission. SID is supported by a Beatriu de Pinós fellowship (2020 BP 00116). SID was supported by MRC grant MR/K004360/1 and a Marie Sklodowska-Curie COFUND EU-UK Research Fellowship.

CONFLICT OF INTEREST

The authors declare no conflicts of interest.

AUTHOR CONTRIBUTIONS

Stavros I. Dimitriadis: conceptualization, methodology, software, validation, formal analysis, investigation, data curation, roles/writing - original draft and funding acquisition.

Eirini Messaritaki: Formal analysis, data curation, Writing–review and editing, funding acquisition.

Resources: The original diffusion MRI are free available from the Human Connectome Project. The analysis of tractography and the construction of structural brain networks has been realised by Eirini Messaritaki.

Derek K. Jones: Writing–review and editing

Bibliography

Atasoy, S., Deco, G., Kringelbach, M.L., Pearson, J., 2018a. Harmonic brain modes: A unifying framework for linking space and time in brain dynamics. Neuroscientist 24, 277–293. doi:10.1177/1073858417728032

Atasoy, S., Donnelly, I., Pearson, J., 2016. Human brain networks function in connectome-specific harmonic waves. Nat. Commun. 7, 10340. doi:10.1038/ncomms10340

Atasoy, S., Roseman, L., Kaelen, M., Kringelbach, M.L., Deco, G., Carhart-Harris, R.L., 2017. Connectome-harmonic decomposition of human brain activity reveals dynamical repertoire re-organization under LSD. Sci. Rep. 7, 17661. doi:10.1038/s41598-017-17546-0

Atasoy, S., Vohryzek, J., Deco, G., Carhart-Harris, R.L., Kringelbach, M.L., 2018b. Common neural signatures of psychedelics: Frequency-specific energy changes and repertoire expansion revealed using connectome-harmonic decomposition. Prog. Brain Res. 242, 97–120. doi:10.1016/bs.pbr.2018.08.009

Atay, F.M., Bıyıkoğlu, T., Jost, J., 2006. Network synchronization: Spectral versus statistical properties. Physica D: Nonlinear Phenomena 224, 35–41. doi:10.1016/j.physd.2006.09.018

Banerjee, A., Jost, J., 2007. Spectral plots and the representation and interpretation of biological data. Theory Biosci. 126, 15–21. doi:10.1007/s12064-007-0005-9

Banerjee, A., Jost, J., 2008. On the spectrum of the normalized graph Laplacian. Linear Algebra Appl. 428, 3015–3022. doi:10.1016/j.laa.2008.01.029

Banerjee, A., Jost, J., 2009. Graph spectra as a systematic tool in computational biology. Discrete Applied Mathematics 157, 2425–2431. doi:10.1016/j.dam.2008.06.033

Banerjee, A., 2012. Structural distance and evolutionary relationship of networks. BioSystems 107, 186–196. doi:10.1016/j.biosystems.2011.11.004

Bassett, D.S., Bullmore, E., 2006. Small-world brain networks. Neuroscientist 12, 512–523. doi:10.1177/1073858406293182

Boccaletti, S., Latora, V., Chavez, M., Hwang, D.U., 2006. Complex networks: Structure and dynamics. Physics Reports 424, 175–308.

doi:10.1016/j.physrep.2005.10.009
Bonacich, P., 1972. Factoring and weighting approaches to status scores and clique identification. J. Math. Sociol. 2, 113–120. doi:10.1080/0022250X.1972.9989806
Bonacich, P., 2007. Some unique properties of eigenvector centrality. Soc. Networks 29, 555–564. doi:10.1016/j.socnet.2007.04.002
Bullmore, E., Sporns, O., 2009. Erratum: Complex brain networks: graph theoretical analysis of structural and functional systems. Nat. Rev. Neurosci. 10, 312–312. doi:10.1038/nrn2618
Bullmore, E., Sporns, O., 2012. The economy of brain network organization. Nat. Rev. Neurosci. 13, 336–349. doi:10.1038/nrn3214
Cheng, X.-Q., Shen, H.-W., 2010. Uncovering the community structure associated with the diffusion dynamics on networks. J. Stat. Mech. 2010, P04024. doi:10.1088/1742-5468/2010/04/P04024
Chung, F.R.K., 1996. Spectral Graph Theory (CBMS Regional Conference Series in Mathematics, No. 92). American Mathematical Society. 1–228.
Collin, G., Sporns, O., Mandl, R.C.W., van den Heuvel, M.P., 2014. Structural and functional aspects relating to cost and benefit of rich club organization in the human cerebral cortex. Cereb. Cortex 24, 2258–2267. doi:10.1093/cercor/bht064
de Lange, S.C., de Reus, M.A., van den Heuvel, M.P., 2014. The Laplacian spectrum of neural networks. Front. Comput. Neurosci. 7, 189. doi:10.3389/fncom.2013.00189
Desikan, R.S., Ségonne, F., Fischl, B., Quinn, B.T., Dickerson, B.C., Blacker, D., Buckner, R.L., Dale, A.M., Maguire, R.P., Hyman, B.T., Albert, M.S., Killiany, R.J., 2006. An automated labeling system for subdividing the human cerebral cortex on MRI scans into gyral based regions of interest. Neuroimage 31, 968–980. doi:10.1016/j.neuroimage.2006.01.021
Destrieux, C., Fischl, B., Dale, A., Halgren, E., 2010. Automatic parcellation of human cortical gyri and sulci using standard anatomical nomenclature. Neuroimage 53, 1–15. doi:10.1016/j.neuroimage.2010.06.010
Dimitriadis, S.I., Antonakakis, M., Simos, P., Fletcher, J.M., Papanicolaou, A.C., 2017a. Data-Driven Topological Filtering Based on Orthogonal Minimal Spanning Trees: Application to Multigroup Magnetoencephalography Resting-State Connectivity. Brain Connect. 7, 661–670. doi:10.1089/brain.2017.0512
Dimitriadis, S.I., Drakesmith, M., Bells, S., Parker, G.D., Linden, D.E., Jones, D.K., 2017b. Improving the Reliability of Network Metrics in Structural Brain Networks by Integrating Different Network Weighting Strategies into a Single Graph. Front. Neurosci. 11, 694. doi:10.3389/fnins.2017.00694
Dimitriadis, S.I., Messaritaki, E., Jones, D.K., 2021. The impact of graph construction scheme and community detection algorithm on the repeatability of community and hub identification in structural brain networks. Human Brain Mapping 42(13), 4261-4280
Dimitriadis, S.I., Routley, B., Linden, D.E., Singh, K.D., 2018. Reliability of Static and Dynamic Network Metrics in the Resting-State: A MEG-Beamformed

Connectivity Analysis. Front. Neurosci. 12, 506. doi:10.3389/fnins.2018.00506
Dimitriadis, S.I., Salis, C., Tarnanas, I., Linden, D.E., 2017c. Topological Filtering of Dynamic Functional Brain Networks Unfolds Informative Chronnectomics: A Novel Data-Driven Thresholding Scheme Based on Orthogonal Minimal Spanning Trees (OMSTs). Front. Neuroinformatics 11, 28. doi:10.3389/fninf.2017.00028
Donetti, L., 2005. Improved spectral algorithm for the detection of network communities, in: AIP Conference Proceedings. Presented at the MODELING COOPERATIVE BEHAVIOR IN THE SOCIAL SCIENCES, AIP, pp. 104–107. doi:10.1063/1.2008598
Estrada, E. The many facets of the Estrada indices of graphs and networks. SeMA 79, 57–125 (2022). https://doi.org/10.1007/s40324-021-00275-w
Feinberg, D.A., Moeller, S., Smith, S.M., Auerbach, E., Ramanna, S., Gunther, M., Glasser, M.F., Miller, K.L., Ugurbil, K., Yacoub, E., 2010. Multiplexed echo planar imaging for sub-second whole brain FMRI and fast diffusion imaging. PLoS ONE 5, e15710. doi:10.1371/journal.pone.0015710
Fortunato, S., 2010. Community detection in graphs. Phys. Rep. 486, 75–174. doi:10.1016/j.physrep.2009.11.002
Glasser, M.F., Sotiropoulos, S.N., Wilson, J.A., Coalson, T.S., Fischl, B., Andersson, J.L., Xu, J., Jbabdi, S., Webster, M., Polimeni, J.R., Van Essen, D.C., Jenkinson, M., WU-Minn HCP Consortium, 2013. The minimal preprocessing pipelines for the Human Connectome Project. Neuroimage 80, 105–124. doi:10.1016/j.neuroimage.2013.04.127
Griffa, A., Amico, E., Liégeois, R., Van De Ville, D., Preti, M.G., 2022. Brain structure-function coupling provides signatures for task decoding and individual fingerprinting. Neuroimage 250, 118970. doi:10.1016/j.neuroimage.2022.118970
Hagmann, P., Cammoun, L., Gigandet, X., Meuli, R., Honey, C.J., Wedeen, V.J., Sporns, O., 2008. Mapping the structural core of human cerebral cortex. PLoS Biol. 6, e159. doi:10.1371/journal.pbio.0060159
Hakimi-Nezhaad, M., Ashrafi, A.R., 2014. A note on normalized Laplacian energy of graphs. J. Contemp. Mathemat. Anal. 49, 207–211. doi:10.3103/S106836231405001X
Harriger, L., van den Heuvel, M.P., Sporns, O., 2012. Rich club organization of macaque cerebral cortex and its role in network communication. PLoS ONE 7, e46497. doi:10.1371/journal.pone.0046497
Huang, W., Bolton, T.A.W., Medaglia, J.D., Bassett, D.S., Ribeiro, A., Van De Ville, D., 2018. A graph signal processing perspective on functional brain imaging. Proc. IEEE 106, 868–885. doi:10.1109/JPROC.2018.2798928
Iturria-Medina, Y., Sotero, R.C., Canales-Rodríguez, E.J., Alemán-Gómez, Y., Melie-García, L., 2008. Studying the human brain anatomical network via diffusion-weighted MRI and Graph Theory. Neuroimage 40, 1064–1076. doi:10.1016/j.neuroimage.2007.10.060

Leemans, A., Jeurissen, B., Sijbers, J., Jones, D.K., 2009. ExploreDTI: a graphical toolbox for processing, analyzing, and visualizing diffusion MR data. ISMRM.

Liang, Z., King, J., Zhang, N., 2011. Uncovering intrinsic connectional architecture of functional networks in awake rat brain. J. Neurosci. 31, 3776–3783. doi:10.1523/JNEUROSCI.4557-10.2011

Luppi, A.I., Vohryzek, J., Kringelbach, M.L., Mediano, P.A.M., Craig, M.M., Adapa, R., Carhart-Harris, R.L., Roseman, L., Pappas, I., Finoia, P., Williams, G.B., Allanson, J., Pickard, J.D., Menon, D.K., Atasoy, S., Stamatakis, E.A., 2020. Connectome Harmonic Decomposition of Human BrainDynamics Reveals a Landscape of Consciousness. biorxiv.

Maslov, S., Sneppen, K., 2002. Specificity and stability in topology of protein networks. Science 296, 910–913. doi:10.1126/science.1065103

McGraw, P.N., Menzinger, M., 2008. Laplacian spectra as a diagnostic tool for network structure and dynamics. Phys. Rev. E Stat. Nonlin. Soft Matter Phys. 77, 031102. doi:10.1103/PhysRevE.77.031102

Medaglia, J.D., Huang, W., Karuza, E.A., Kelkar, A., Thompson-Schill, S.L., Ribeiro, A., Bassett, D.S., 2018. Functional Alignment with Anatomical Networks is Associated with Cognitive Flexibility. Nat. Hum. Behav. 2, 156–164. doi:10.1038/s41562-017-0260-9

Messaritaki, E., Dimitriadis, S.I., Jones, D.K., 2019. Optimization of graph construction can significantly increase the power of structural brain network studies. Neuroimage 199, 495–511. doi:10.1016/j.neuroimage.2019.05.052

Moeller, S., Yacoub, E., Olman, C.A., Auerbach, E., Strupp, J., Harel, N., Uğurbil, K., 2010. Multiband multislice GE-EPI at 7 tesla, with 16-fold acceleration using partial parallel imaging with application to high spatial and temporal whole-brain fMRI. Magn. Reson. Med. 63, 1144–1153. doi:10.1002/mrm.22361

Naze, S., Proix, T., Atasoy, S., Kozloski, J.R., 2021. Robustness of connectome harmonics to local gray matter and long-range white matter connectivity changes. Neuroimage 224, 117364. doi:10.1016/j.neuroimage.2020.117364

Newman, M.E.J., 2006. Modularity and community structure in networks. Proc Natl Acad Sci USA 103, 8577–8582. doi:10.1073/pnas.0601602103

Newman, M., 2003. The Structure and Function of Complex Networks. SIAM Rev. 45, 167–256. doi:10.1137/S003614450342480

Page, L., Brin, S., Rajeev, M., Terry, W., 2001. The PageRank Citation Ranking: Bringing Order to the Web. Technical Report 1, 1999–1966.

Preti, M.G., Van De Ville, D., 2019. Decoupling of brain function from structure reveals regional behavioral specialization in humans. Nat. Commun. 10, 4747. doi:10.1038/s41467-019-12765-7

Raj, A., Kuceyeski, A., Weiner, M., 2012. A network diffusion model of disease progression in dementia. Neuron 73, 1204–1215. doi:10.1016/j.neuron.2011.12.040

Rubner, Y., 2000. :{unav). Springer Science and Business Media LLC. doi:10.1023/a:1026543900054

Setsompop, K., Gagoski, B.A., Polimeni, J.R., Witzel, T., Wedeen, V.J., Wald, L.L.,

2012. Blipped-controlled aliasing in parallel imaging for simultaneous multislice echo planar imaging with reduced g-factor penalty. Magn. Reson. Med. 67, 1210–1224. doi:10.1002/mrm.23097

Shen, H.-W., Cheng, X.-Q., 2010. Spectral methods for the detection of network community structure: a comparative analysis. J. Stat. Mech. 2010, P10020. doi:10.1088/1742-5468/2010/10/P10020

Shi, J., Malik, J., 2000. Normalized cuts and image segmentation. IEEE Trans. Pattern Anal. Mach. Intell. 22, 888–905. doi:10.1109/34.868688

Sihag, S., Naze, S., Taghdiri, F., Tator, C., Wennberg, R., Mikulis, D., Green, R., Colella, B., Tartaglia, M.C., Kozloski, J.R., 2020. Multimodal Dynamic Brain Connectivity Analysis Based on Graph Signal Processing for Former Athletes with History of Multiple Concussions. IEEE Trans. on Signal and Inf. Process. over Networks 1–1. doi:10.1109/TSIPN.2020.2982765

Sotiropoulos, Stamatios N, Jbabdi, S., Xu, J., Andersson, J.L., Moeller, S., Auerbach, E.J., Glasser, M.F., Hernandez, M., Sapiro, G., Jenkinson, M., Feinberg, D.A., Yacoub, E., Lenglet, C., Van Essen, D.C., Ugurbil, K., Behrens, T.E.J., WU-Minn HCP Consortium, 2013. Advances in diffusion MRI acquisition and processing in the Human Connectome Project. Neuroimage 80, 125–143. doi:10.1016/j.neuroimage.2013.05.057

Sotiropoulos, S N, Moeller, S., Jbabdi, S., Xu, J., Andersson, J.L., Auerbach, E.J., Yacoub, E., Feinberg, D., Setsompop, K., Wald, L.L., Behrens, T.E.J., Ugurbil, K., Lenglet, C., 2013. Effects of image reconstruction on fiber orientation mapping from multichannel diffusion MRI: reducing the noise floor using SENSE. Magn. Reson. Med. 70, 1682–1689. doi:10.1002/mrm.24623

Sporns, O., and Kötter, R. (2004). Motifs in brain networks. PLoS Biol. 2:e369. doi: 10.1371/journal.pbio.0020369

Tournier, J.-D., Calamante, F., Gadian, D.G., Connelly, A., 2004. Direct estimation of the fiber orientation density function from diffusion-weighted MRI data using spherical deconvolution. Neuroimage 23, 1176–1185. doi:10.1016/j.neuroimage.2004.07.037

Trefler A, Neda Sadeghi, Adam G. Thomas, Carlo Pierpaoli, Chris I. Baker, Cibu Thomas, Impact of time-of-day on brain morphometric measures derived from T1-weighted magnetic resonance imaging, NeuroImage, 133, 2016, 41-52,

Tzourio-Mazoyer, N., Landeau, B., Papathanassiou, D., Crivello, F., Etard, O., Delcroix, N., Mazoyer, B., Joliot, M., 2002. Automated anatomical labeling of activations in SPM using a macroscopic anatomical parcellation of the MNI MRI single-subject brain. Neuroimage 15, 273–289. doi:10.1006/nimg.2001.0978

van den Heuvel, M.P., Hulshoff Pol, H.E., 2010. Specific somatotopic organization of functional connections of the primary motor network during resting state. Hum. Brain Mapp. 31, 631–644. doi:10.1002/hbm.20893

van den Heuvel, M.P., Sporns, O., 2013a. Network hubs in the human brain. Trends Cogn Sci (Regul Ed) 17, 683–696. doi:10.1016/j.tics.2013.09.012

van den Heuvel, M.P., Sporns, O., 2013b. An anatomical substrate for integration

among functional networks in human cortex. J. Neurosci. 33, 14489–14500. doi:10.1523/JNEUROSCI.2128-13.2013

van den Heuvel, M.P., Stam, C.J., Boersma, M., Hulshoff Pol, H.E., 2008. Small-world and scale-free organization of voxel-based resting-state functional connectivity in the human brain. Neuroimage 43, 528–539. doi:10.1016/j.neuroimage.2008.08.010

Van Essen, D.C., Smith, S.M., Barch, D.M., Behrens, T.E.J., Yacoub, E., Ugurbil, K., WU-Minn HCP Consortium, 2013. The WU-Minn Human Connectome Project: an overview. Neuroimage 80, 62–79. doi:10.1016/j.neuroimage.2013.05.041

Varshney, L.R., Chen, B.L., Paniagua, E., Hall, D.H., Chklovskii, D.B., 2011. Structural properties of the Caenorhabditis elegans neuronal network. PLoS Comput. Biol. 7, e1001066. doi:10.1371/journal.pcbi.1001066

Vukadinović, D., Huang, P., Erlebach, T., 2002. On the spectrum and structure of internet topology graphs, in: Unger, H., Böhme, T., Mikler, A. (Eds.), Innovative Internet Computing Systems, Lecture Notes in Computer Science. Springer Berlin Heidelberg, Berlin, Heidelberg, pp. 83–95. doi:10.1007/3-540-48080-3_8

Wang, M.B., Owen, J.P., Mukherjee, P., Raj, A., 2017. Brain network eigenmodes provide a robust and compact representation of the structural connectome in health and disease. PLoS Comput. Biol. 13, e1005550. doi:10.1371/journal.pcbi.1005550

Welton, T., D.A. Kent, D.P. Auer, R.A. Dineen.Reproducibility of graph-theoretic brain network metrics: a systematic review.Brain Connect., 5 (4) (2015), pp. 193-202

Xu, J., Moeller, S., Strupp, J., Auerbach, E., Chen, L., Feinberg, D.A., Ugurbil, K., Yacoub, E., 2012. Highly accelerated whole brain imaging using aligned-blipped-controlled-aliasing multiband EPI. Proc. Int. Soc. Mag. Reson. Med 20, 2306.